Pressure dependence of superconductivity in low- and high-T_c phases of $(NH_3)_yNa_xFeSe$

Takahiro Terao,[1] Xiaofan Yang,[1] Xiao Miao,[1] Lu Zheng,[1] Hidenori Goto,[1] Takafumi Miyazaki,[2] Hitoshi Yamaoka,[3] Hirofumi Ishii,[4] Yen-Fa Liao,[4] and Yoshihiro Kubozono[1,*]

[1]*Research Institute for Interdisciplinary Science, Okayama University, Okayama 700–8530, Japan*

[2]*Research Laboratory for Surface science, Okayama University, Okayama 700–8530, Japan*

[3]*RIKEN SPring-8 Center, Hyogo 679–5148, Japan*

[4]*National Synchrotron Radiation Research Center, Hsinchu 30076, Taiwan*

(Received 11 November 2017; revised manuscript received 23 January 2018; published 9 March 2018)

We prepared two superconducting phases, which are called "low-T_c phase" and "high-T_c phase" of $(NH_3)_yNa_xFeSe$ showing T_c's of 35 and 44 K, respectively, at ambient pressure, and studied the superconducting behavior and structure of each phase under pressure. The T_c of the 35 K at ambient pressure rapidly decreases with increasing pressure up to 10 GPa, and it remains unchanged up to 22 GPa. Finally, superconductivity was not observed down to 1.4 K at 29 GPa, i.e., $T_c < 1.4$ K. The T_c of the 44 K phase also shows a monotonic decrease up to 15 GPa and it weakly decreases up to 25 GPa. These behaviors suggest no pressure-driven high-T_c phase (called "SC-II") between 0 and 25 GPa for the low-T_c and high-T_c phases of $(NH_3)_yNa_xFeSe$, differing from the behavior of $(NH_3)_yCs_xFeSe$, which has a pressure-driven high-T_c phase (SC-II) in addition to the superconducting phase (SC-I) observed at ambient and low pressures. The T_c-c phase diagram for both low-T_c and high-T_c phases shows that the T_c can be linearly scaled with c (or FeSe plane spacing), where c is a lattice constant. The reason why a pressure-driven high-T_c phase (SC-II) was found for neither low-T_c nor high-T_c phases of $(NH_3)_yNa_xFeSe$ is fully discussed, suggesting a critical c value as the key to forming the pressure-driven high-T_c phase (SC-II). Finally, the precise T_c-c phase diagram is depicted using the data obtained thus far from FeSe codoped with a metal and NH_3 or amine, indicating two distinct T_c-c lines below $c = 17.5$ Å.

DOI: 10.1103/PhysRevB.97.094505

I. INTRODUCTION

The pressure dependence of superconductivity in various metal-intercalated two-dimensional (2D) layered materials has been extensively studied in past decades [1–10]. The exciting behavior of a superconducting transition temperature T_c that varies with pressure (p) was observed in superconducting $K_{0.8}Fe_{1.7}Se_2$, $K_{0.8}Fe_{1.78}Se_2$ and $Tl_{0.6}Rb_{0.4}Fe_{1.67}Se_2$ crystals, which showed a double-dome superconductivity with pressure [1]. These metal-doped FeSe materials exhibited T_c values as high as ∼30 K at 0 GPa [11–14]. T_c values of 48.0–48.7 K were recorded at pressures above 10 GPa, despite a monotonic decrease in T_c from ∼30 K at 0 GPa with applied pressure [1]. The pressure-driven high-T_c phase is called "superconducting phase II (SC-II)," while the low-pressure phase is "superconducting phase I (SC-I)." Subsequently, a pressure-induced quantum critical transition was investigated in $K_{0.8}Fe_xSe_2$ using x-ray powder diffraction and electrical transport under high pressure [2]. This study found the transitions in the pressure range of 9.2–10.3 GPa, which refer to the transitions (1) from metallic Fermi liquid (FL) to non-Fermi liquid (NFL) behavior and (2) from antiferromagnetic (AFM) to paramagnetic (PM) states. The former transition was confirmed from the normal state resistance (R), as evidenced in the change of α in the expression $\rho = \rho_0 + AT^\alpha$ from 2.7 at ambient pressure to 1 above 9–10 GPa. Furthermore, a ^{57}Fe Mössbauer study of $Rb_{0.8}Fe_{1.6}Se_{2.0}$ revealed the appearance of a new magnetic phase above 5 GPa [3]. Strictly speaking, the AFM phase coexisted with FL behavior at low pressure, and the AFM phase was assigned to the 245 superlattice structure of Fe vacancies, as found in the superconducting M_xFeSe (M: metal atom) sample, i.e., the superconducting phase coexisted with the AFM phase at a nanoscale phase separation [15–18].

The role of the 245 AFM phase in superconductivity was fully investigated using the R-T plots of antiferromagnetic $Tl_{0.36}Rb_{0.44}Fe_{1.56}Se_2$ and $K_{0.8}Fe_{1.60}Se_2$ phases as well as those of superconducting $Tl_{0.4}Rb_{0.4}Fe_{1.67}Se_2$ and $K_{0.6}Fe_{1.70}Se_2$ phases, at different pressures from 0 to 22 GPa [4], which suggested a correlation between the Mott-insulating (MI) phase found in the AFM phase and the SC-I phase. In fact, the SC-I phase completely disappears when the MI phase vanishes, indicating that the SC-I phase may be stabilized by the 245 AFM phase. On the other hand, the SC-II phase appears in the presence of the paramagnetic state and the metallic NFL state, implying no correlation between the AFM phase and SC-II. Furthermore, the pressure dependence of T_c was extensively studied in metal-doped $FeSe_{2-x}Te_x$ with different x's [5], in which phase diagrams similar to that of metal-doped FeSe (or $x = 0$) were found, i.e., a double-dome superconducting phase consisting of SC-I and SC-II was confirmed for $x \neq 0$, although the maximum T_c values for both superconducting phases when $x \neq 0$ become lower than those for $x = 0$. This study stresses the correlation of SC-I with a long-range ordered AFM state and the re-emergence of SC-II with a pressure-induced AFM fluctuation state [5].

*Corresponding author: kubozono@cc.okayama-u.ac.jp

In addition, pure FeSe [6] and topological materials [7–10] also provided high-T_c superconducting phases under pressure. Thus the pressure dependence of superconductivity for metal-doped two-dimensional materials described above has been an exciting research subject.

The pressure dependence of superconductivity was also investigated for ammoniated Cs-doped FeSe, $(NH_3)_yCs_{0.4}FeSe$ [19], which exhibited a T_c value as high as 31 K at 0 GPa [20]. A double-dome T_c-p phase diagram was observed for $(NH_3)_yCs_{0.4}FeSe$. The T_c gradually decreased with increasing pressure up to 13 GPa, and a T_c re-emerged suddenly at 15 GPa, i.e., SC-II emerged. The T_c in the SC-II phase reached 49 K at 21 GPa. In the case of ammoniated metal-doped FeSe, the pressure dependence of superconductivity was investigated using a polycrystalline powder sample, and the role of the AFM phase has not been discussed. It has been found from these results that the emergence of pressure-driven high-T_c phase (SC-II) may be a common feature in ammoniated metal doped FeSe.

Recently, some research groups have prepared various types of ammoniated metal-doped FeSe, $(NH_3)_yM_xFeSe$ (M: metal atom), using liquid NH_3 [20–23]. Among these, it was found that $(NH_3)_yNa_xFeSe$ provided multiple superconducting phases [22,23]; the x dependence of T_c and c in $(NH_3)_yNa_xFeSe$ is fully reported in Ref. [22], providing only two phases (low-T_c and high-T_c phases) at 0 GPa. The smaller (larger) x in $(NH_3)_yNa_xFeSe$ provides lower (higher) T_c and smaller (larger) c value. Namely, studying the pressure dependence of T_c and c (called as "study on physical pressure effect") using these two phases is significant to systematically clarify the correlation between T_c and c. Furthermore, it is very interesting to pursue whether both low-T_c and high-T_c phases show the pressure-driven high-T_c phase (SC-II). Based on the study of various $(NH_3)_yM_xFeSe$, it was concluded that the T_c can be well scaled with the lattice constant c (or FeSe plane spacing) [24], in which case, the T_c increases with increasing c up to ~17 Å, and gradually decreases with further increase in c. This leads to the study of the chemical pressure effect of c on T_c. This behavior is also established in $(NH_3)_yM_xFeSe_{0.5}Te_{0.5}$ [25]. To sum up, the study of the physical pressure effect is indispensable for both phases of $(NH_3)_yNa_xFeSe$.

Here, we report the pressure dependence of superconductivity and crystal structure in two phases ($T_c = 35$ K and $T_c = 44$ K at 0 GPa) of $(NH_3)_yNa_xFeSe$, which are called "low-T_c and high-T_c phases," respectively. The purpose of this study is (1) to clarify the difference in the pressure dependence of superconductivity between the two phases, and (2) to show the precise T_c-c phase diagram for the pressure dependence of T_c and the crystal structure. The study of the pressure dependence of superconductivity and crystal structure of both phases in $(NH_3)_yNa_xFeSe$ must lead to answers for questions on not only the correlation between T_c and c but also the emergence of pressure-driven high-T_c phase (SC-II), by combining with the experimental data reported thus far [physical pressure effect in $(NH_3)_yCs_xFeSe$ and chemical pressure effect in $(NH_3)_yM_xFeSe$] [19–22]. Through such study, we also pursue the mechanism of the emergence of superconductivity in M_xFeSe.

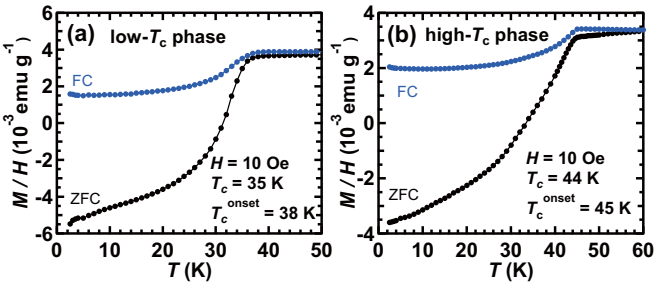

FIG. 1. M/H vs T plots for (a) low-T_c and (b) high-T_c phases of $(NH_3)_yNa_xFeSe$ (ZFC and FC modes) at ambient pressure; nominal x values were 0.4 and 0.7, respectively, for the low-T_c and high-T_c phases. Applied H was 10 Oe.

II. METHODS

The samples of $(NH_3)_yNa_xFeSe$ were prepared according to the method described in the previous paper [20]. The XRD patterns of samples under pressure were measured at 297 K, using synchrotron radiation at BL12B2 of SPring-8; the wavelength λ of the x-ray beam was 0.6889 Å. A diamond anvil cell (DAC) was used for the high-pressure XRD measurement; the sample was loaded into the hole of an SUS plate. The pressure medium daphne 7373 was used for the XRD measurement under high pressure. The pressure was determined by monitoring ruby fluorescence. The superconductivity of the $(NH_3)_yNa_xFeSe$ samples was checked at 0–1.1 GPa using the dc magnetic susceptibility (M/H) recorded by a SQUID magnetometer (Quantum Design MPMS2); the pressure medium daphne 7373 was also used in the pressure-dependent M/H measurement; M and H refer to magnetization and applied magnetic field, respectively.

The temperature dependence of R was measured in a four-terminal measurement mode under pressure. The $(NH_3)_yNa_xFeSe$ samples were introduced into the DAC in an Ar-filled glove box so as to apply the pressure on the sample without any exposure to air. The sample was loaded directly on a Kapton sheet / epoxy resin / rhenium in the DAC; six Cu electrodes were attached to the Kapton sheet, and this cell was used for measuring the R of the sample. The applied pressure was determined by monitoring ruby fluorescence. The R of the sample was measured in standard four-terminal measurement mode using an Oxford superconducting magnet system; the temperature was regulated using an Oxford Instruments MercuryiTC, and the H was controlled using Oxford Instruments MercuryiPS. Electric current (I) was supplied by a Keithley 220 programmable current source, and the voltage (V) was measured by an Agilent 34420 digital nanovoltmeter. All the measurements are conducted on polycrystalline powder samples but single crystals.

III. RESULTS

Figures 1(a) and 1(b) show the temperature dependence of dc magnetic susceptibility (M/H) in zero field cooling (ZFC) and field cooling (FC) modes for samples of low-T_c and high-T_c phases in $(NH_3)_yNa_xFeSe$. The nominal x value was 0.4

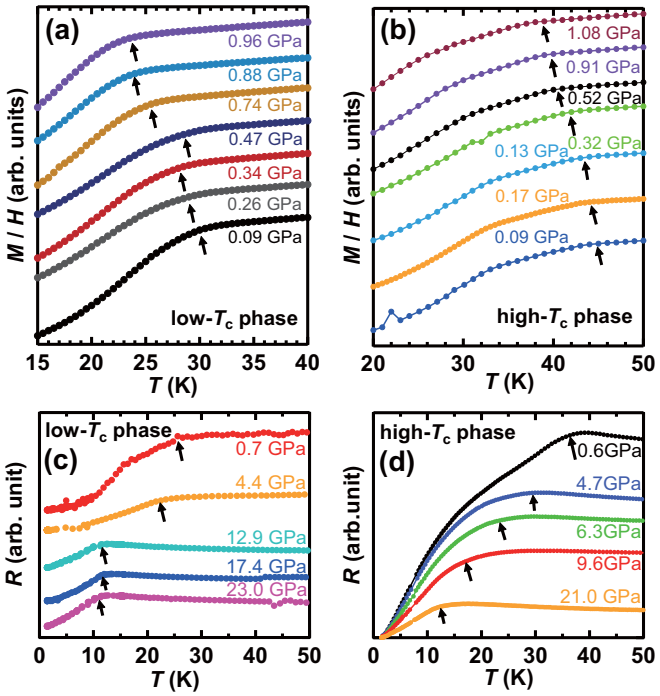

FIG. 2. M/H vs T plots for (a) low-T_c and (b) high-T_c phases of $(NH_3)_yNa_xFeSe$ (ZFC mode) at different pressures; nominal x values were 0.5 and 0.6, respectively, for the low-T_c and high-T_c phases. Applied H was 10 Oe. R-T plots for (c) low-T_c and (d) high-T_c phases of $(NH_3)_yNa_xFeSe$ at different pressures; nominal x values were 0.4 for both the low-T_c and high-T_c phases. The arrows indicate the T_c values. How to determine the T_c is described in the text.

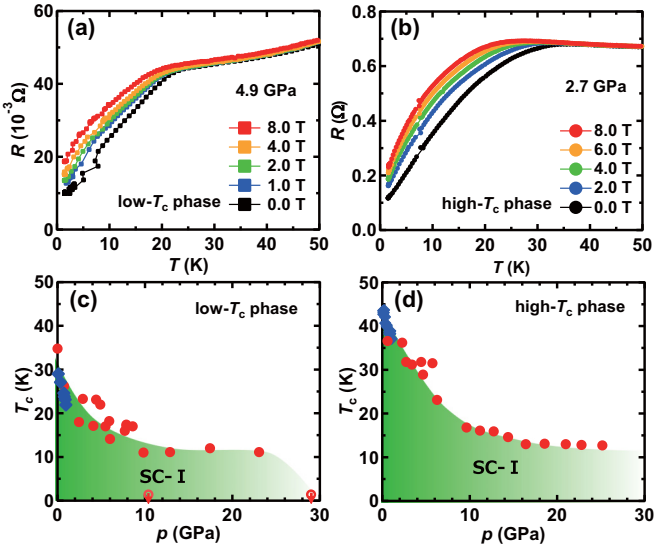

FIG. 3. R-T plots at different H's (0–8.0 T) for (a) low-T_c and (b) high-T_c phases of $(NH_3)_yNa_xFeSe$; nominal x values were 0.4 for both the low-T_c and high-T_c phases. Pressures of 4.9 and 2.7 GPa were applied in (a) and (b), respectively. T_c-p phase diagrams of (c) low-T_c and (d) high-T_c phases of $(NH_3)_yNa_xFeSe$. The blue diamonds and red circles refer to the T_c values determined from M/H-T and R-T plots, respectively. Open red circles for the low-T_c phase represent the cases in which no superconducting transition was observed. The T_c-p phase diagrams [(c) and (d)] were based on measurements made on two samples for low-T_c phase and three samples for high-T_c phase.

and 0.7, respectively, for the samples of low-T_c and high-T_c phases. A clear superconducting transition was observed in both phases, with T_c^{onset} and T_c of 38 and 35 K, respectively, in ZFC mode for the low-T_c phase, and 45 and 44 K, respectively, in ZFC mode for the high-T_c phase; the T_c was determined from the crossing point of flat M/H-T plot (normal state) and the drop of M/H-T plot observed at ZFC mode, while the T_c^{onset} refers to the onset temperature providing the deviation from the flat M/H-T plot (normal state) at ZFC mode. These values are consistent with those reported previously [22]. As described later, these samples contain other phases such as pure β-FeSe and Fe_7Se_8, but the above T_c^{onset} and T_c definitely correspond to the low-T_c and high-T_c phases. The shielding fraction at 2.5 K was 48% and 33%, respectively, for the low-T_c and high-T_c phases. The shielding fraction was evaluated from the M/H-T plot at ZFC mode. It was evident from these results that both the low-T_c and high-T_c phases in $(NH_3)_yNa_xFeSe$ could be prepared.

The M/H versus T plots of the low-T_c and high-T_c phases in $(NH_3)_yNa_xFeSe$ samples measured at different pressures (0–1.1 GPa) are shown in Figs. 2(a) and 2(b), where it is clear that the plots gradually shift to the left with increasing pressure; the T_c value was definitely determined from each M/H-T plot by the same way as that described above. Figures 2(c) and 2(d) depict the temperature dependence of resistance (R-T plots) for the low-T_c and high-T_c phases in $(NH_3)_yNa_xFeSe$ measured at different pressures. The temperature for R drop shifts to the left with increasing pressure, i.e., the T_c's for both phases decrease monotonically; the T_c value was definitely determined from the crossing point between the flat R-T plot and the drop of R-T plot. The T_c's determined from M/H-T and R-T plots refer to the superconducting transition temperature for the main phase contained in each sample, which is called low-T_c or high-T_c phase.

Figures 3(a) and 3(b) show the R-T plots for the low-T_c and high-T_c phases in $(NH_3)_yNa_xFeSe$ measured under applied H. The applied pressures were 4.9 and 2.7 GPa, respectively, for the low-T_c and high-T_c phases. Applying H gradually suppressed the R drop, indicating that the R drops observed for both phases can be assigned to a superconducting transition. Here, it is noticed that the complete zero-R could not be recorded in Figs. 3(a) and 3(b), because the sample is a polycrystalline powder, which has still resistance at grain boundaries. Nevertheless, the suppression of the R drop by applied H absolutely guarantees the superconducting transition.

The T_c-p plots for the low-T_c and high-T_c phases in $(NH_3)_yNa_xFeSe$ are shown in Figures 3(c) and 3(d), which were prepared based on the M/H-T and R-T plots at different pressures. The T_c-p plots for both phases did not show an emergence of the high-pressure driven superconducting phase (SC-II), i.e., only SC-I was observed at 0–25 GPa, which is different from the T_c-p phase diagram previously reported for metal-doped FeSe [1,19], indicating that the emergence of a pressure-driven high-T_c superconducting phase is not a universal phenomenon for metal-doped FeSe. This leads to the question of why such a different T_c-p behavior is observed in $(NH_3)_yNa_xFeSe$, which is addressed in the discussion section.

The XRD patterns of the samples of low-T_c and high-T_c phases measured under pressure are shown in Figs. 4(a) and 4(b). The peaks observed for both phases smoothly shift to higher 2θ values with increasing pressure. The XRD pattern for the sample of low-T_c phase at 0 GPa could be reproduced by the combination of three phases, low-T_c phase, β-FeSe, and Fe_7Se_8. The main peaks at 0 GPa were assigned to the low-T_c phase (major phase) and β-FeSe (minor phase). On the other hand, the XRD pattern for the sample of the high-T_c phase could be reproduced by the three phases of high-T_c phase (major phase), low-T_c phase (minor phase), and Fe_7Se_8. A small amount of Fe_7Se_8 is contained in both samples. Thus each sample of low-T_c and high-T_c phases contains the corresponding phase as a major phase.

With increasing pressure, the peaks observed broaden and overlap. Therefore it was difficult to carry out LeBail or Rietveld refinement in order to determine the lattice constants. Consequently, the lattice constant c was determined from only the 002 peak for both phases, because the 002 peak is not overlapped by other peaks. Actually, we could achieve LeBail fitting for the XRD patterns at ambient and low pressures, and the c values at low pressures determined by LeBail fitting were close to those determined from the 002 peak. Namely, the c values were 13.537 and 13.548(4) Å for the low-T_c phase determined from the 002 peak and LeBail fitting at 0 GPa, respectively, while those were 17.151 and 17.07(3) Å for the high-T_c phase determined from the 002 peak and LeBail fitting at 0 GPa, respectively; each sample was set in a DAC for the measurement at 0 GPa. Therefore, at the present stage, the c values obtained from the 002 peak are sufficiently for the discussion of the T_c-c plot. The complete LeBail and Rietveld refinements for all XRD patterns at 0–25 GPa may be part of future work. The values of c for the low-T_c and high-T_c phases at 0 GPa were lower by 0.5−0.7 Å than the previously reported 14.257 Å for the low-T_c phase and 17.565 Å for the high-T_c phase [22]. This may be due to the fact that the sample is under weak pressure because the sample is set in a DAC even for the measurement of XRD patterns at 0 GPa, differently from the measurement in the previous report [22].

The a values were 3.868 and 3.737 Å, respectively, for the low-T_c and high-T_c phases, values that are consistent with those previously reported (3.889 Å for low-T_c phase and 3.826 Å for high-T_c phase [22]). The a value was evaluated from c and the 101 peak for the low-T_c phase, and c and the 103 peak for the high-T_c phase. The a and c values for both phases show a monotonic decrease against pressure, as seen in Figs. 4(c) and 4(d). The a and c for the low-T_c phase were evaluated up to 31 GPa, while those for the high-T_c phase were evaluated only up to 17 GPa because of the progressive disappearance of 002 and 103 peaks. The monotonic decrease suggests the absence of structural phase transitions from 0–31 GPa for the

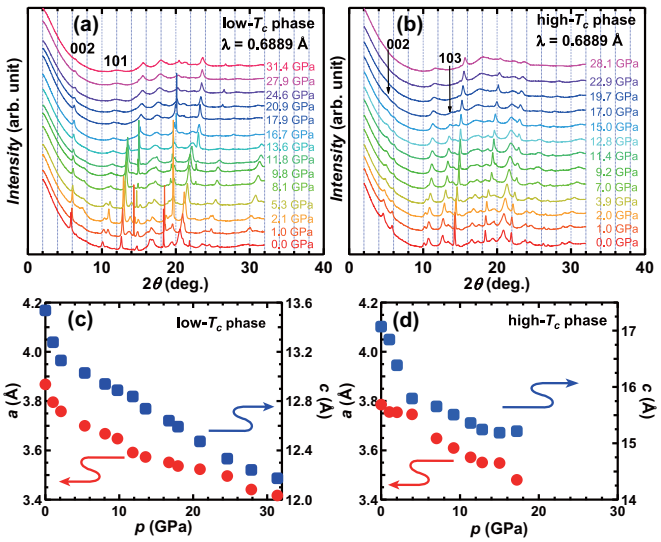

FIG. 4. Pressure-dependent XRD patterns for (a) low-T_c and (b) high-T_c phases of $(NH_3)_yNa_xFeSe$; nominal x values were 0.4 and 0.7, respectively, for the low-T_c and high-T_c phases. A synchrotron x-ray beam of $\lambda = 0.6889$ Å was used to obtain the XRD pattern. The pressure dependence of lattice constants (a and c) for (c) low-T_c and (d) high-T_c phases is plotted as a function of pressure.

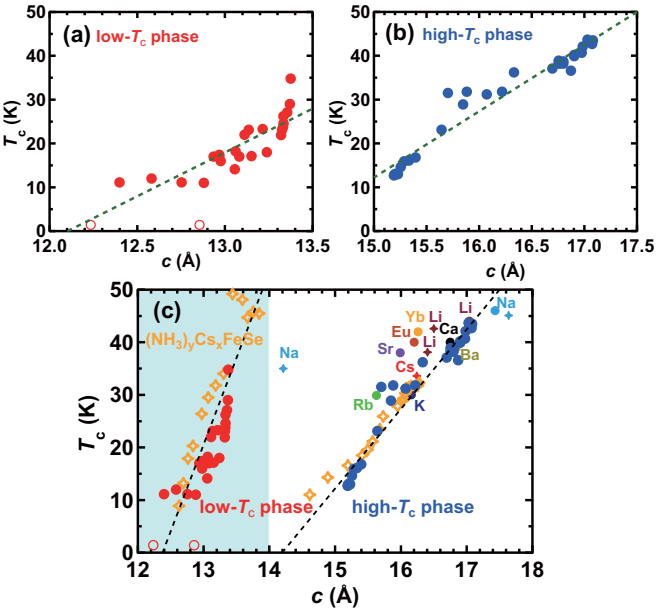

FIG. 5. (a) T_c-c plot for the low-T_c phase of $(NH_3)_yNa_xFeSe$ evaluated from the plots of T_c-p [Fig. 3(c)] and c-p [Fig. 4(c)]. (b) T_c-c plot for the high-T_c phase of $(NH_3)_yNa_xFeSe$ evaluated from the plots of T_c-p [Fig. 3(d)] and c-p [Fig. 4(d)]. Details are as follows: (1) from the experimental c-p plots (Fig. 4), the c-p curves in the entire pressure range were obtained by the interpolation with a single exponential function. (2) Complete T_c-c plots were drawn by comparing the c-p curves and T_c-p plots. Linear relationships in (a) and (b) are shown by dashed lines, which are obtained by a least-squares fitting for data. (c) T_c-c plots for ammoniated M_xFeSe. Red and blue circles refer to the low-T_c and high-T_c phases of $(NH_3)_yNa_xFeSe$ shown in (a) and (b), respectively. Other solid circles and stars (various colors) refer to the T_c-c plots for various ammoniated metal-doped FeSe (see text), and open stars (orange color) refer to the T_c-c plot obtained from the pressure effect on T_c and c in $(NH_3)_yCs_xFeSe$ (see text). The area filled by thin blue color refers to the SC-II phase of $(NH_3)_yCs_xFeSe$, while the area without color refers to the SC-I phase of $(NH_3)_yCs_xFeSe$ and the T_c-c range of various $(NH_3)_yM_xFeSe$ at 0 GPa. Eye guides are depicted by dashed lines (see text).

low-T_c phase, and no structural phase transition up to 17 GPa for the high-T_c phase. These results imply no structural phase transition and no emergence of SC-II in the pressure range achieved in this study, indicating that the physical behavior of SC-I was fully explored in this study.

The T_c-c plots for the low-T_c and high-T_c phases are shown in Figs. 5(a) and 5(b), which demonstrate the linear relationship between T_c and c. Strictly speaking, the T_c-c plot for the high-T_c phase is fitted by a linear relationship, while that for the low-T_c phase is roughly followed by the linear relationship. In other words, the T_c can be substantially scaled with c (or FeSe plane spacing), i.e., the T_c increases with increasing c. This behavior is found in both phases. The T_c-c plot for $(NH_3)_yCs_xFeSe$ [19] and the values of T_c and c for various ammoniated metal-doped FeSe materials [20–22,24] are plotted together with the T_c-c plots for the low-T_c and high-T_c phases in $(NH_3)_yNa_xFeSe$ [Fig. 5(c)]. This clearly provides two different T_c-c lines. As seen from Fig. 5(c), the T_c-c plot for the high-T_c phase in $(NH_3)_yNa_xFeSe$ lies on the T_c-c plot for the SC-I phase of $(NH_3)_yCs_xFeSe$ (physical pressure effect) and those of various ammoniated metal-doped FeSe materials (chemical pressure effect). On the other hand, the T_c-c plot for the low-T_c phase in $(NH_3)_yNa_xFeSe$ lies on the T_c-c plot for the SC-II phase of $(NH_3)_yCs_xFeSe$; the area of SC-II phase is filled by thin blue color in the T_c-c phase diagram of Fig. 5(c). Thus the T_c increases up to 46 K in SC-I, while it increases up to 49 K in SC-II. Very recently, Shahi *et al.* reported pressure-driven superconductivity in $(NH_3)_yLi_xFeSe$, with the highest T_c being 55 K in SC-II [26]. This may also lie on the T_c-c plot for SC-II. The increase in T_c with c is suggested for metal-doped HfNCl [27,28]. The enhancement of T_c against c will be fully addressed in the discussion section.

Finally, the T_c-c phase diagram over a wide c range is shown in Fig. 6. In this phase diagram, the T_c values for metal-doped FeSe's prepared using amine solvents [ethylenediamine (EDA) and hexamethylenediamine (HMDA)], which have a more extended FeSe layer distance than that in ammoniated M_xFeSe's, are plotted; the T_c values for $(AM)_yM_x$FeSe's (AM: EDA or HMDA) are taken from Refs. [25,29–31]. This T_c-c phase diagram provides the complete trend of T_c against c in metal-doped FeSe. The important points in this phase diagram can be summarized as follows. (1) The T_c can be scaled with c up to ~17.5 Å, and the discontinuous jump between SC-I and SC-II is found at $c \sim 14$ Å. (2) The maximum T_c appears at $c \sim 17.5$ Å, and it decreases slowly to reach the T_c (~40 K) for the superconductivity observed in a single layer of FeSe [32]. This behavior is also considered in the discussion section.

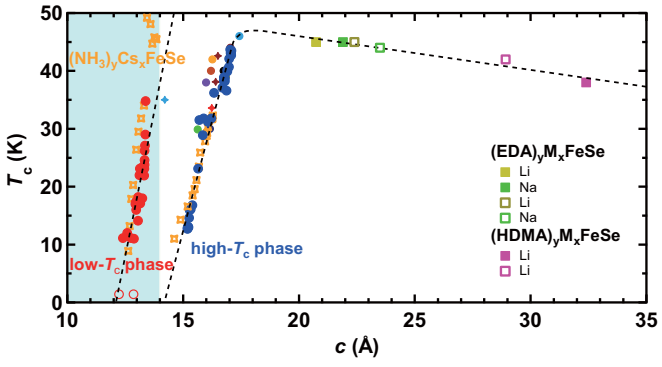

FIG. 6. Precise T_c-c phase diagram of M_xFeSe obtained from ammoniated M_xFeSe and amine/metal-doped FeSe. The T_c-c plot for amine/metal doped FeSe is added to the T_c-c plots shown in Fig. 5(c); details are described in the text. The area filled by thin blue color refers to the SC-II phase of $(NH_3)_yCs_xFeSe$, while the area without color refers to the SC-I phase of $(NH_3)_yCs_xFeSe$ and the T_c-c range of various $(NH_3)_yM_x$FeSe and $(AM)_yM_x$FeSe at 0 GPa. Dashed lines provide eye guides (see text).

IV. DISCUSSION

The reason why the SC-II phase was not found from the pressure dependence of T_c for the low-T_c and high-T_c phases of $(NH_3)_yNa_xFeSe$ [Figs. 3(c) and 3(d)] must be discussed. Recently, studies of the pressure dependence of superconductivity in M_xFeSe [1] and ammoniated M_xFeSe [19,26] showed the presence of SC-II under high pressure. As described in Introduction, changes of the electronic state (FL to NFL) and magnetic state (AFM to PM) were found for M_xFeSe [1]. Furthermore, the structural change accompanied by the transition from SC-I to SC-II has also been reported [33], i.e., the transition from tetragonal to collapsed tetragonal structure was found to occur in $(NH_3)_yCs_xFeSe$ at 8 K, although such a transition was not observed at room temperature [19]. A study of the pressure-dependent Hall effect in $(NH_3)_yLi_xFeSe$ showed a clear correlation between T_c and electron density [26], i.e., a higher T_c is obtained when a higher electron density is produced by higher pressure. Thus the SC-II phase may form due to a rapid increase in electron density accompanied by a sudden change in the Fermi surface topology (or Lifshitz transition) [26]. Furthermore, a recent study of superconductivity from the K dosing of $(Li_{0.8}Fe_{0.2}OH)FeSe$ showed the emergence of a Lifshitz transition due to the crossing of the Γ-centred electron band to Fermi level caused by electron doping [34], which provided a small superconducting gap for $(Li_{0.8}Fe_{0.2}OH)FeSe$. Considering the structural transition of a tetragonal to a collapsed tetragonal structure observed at a pressure corresponding to the SC-I–SC-II transition in $(NH_3)_yCs_xFeSe$ [33], the Lifshitz transition may be directly related to the structural change or shrinkage of the lattice. Actually, such a modification of the Fermi surface topology (or Lifshitz transition) is unambiguously caused by structural distortion, as evidenced in Fe-based superconductors [35].

Our study of the pressure dependence of XRD patterns showed no structural phase transition at 297 K (Fig. 4), but the pressure-dependent XRD pattern was not measured at low temperature. Therefore we cannot know whether both phases of $(NH_3)_yNa_xFeSe$ display any structural change at low temperature, but if such a structural change happens at high pressure, a topological change in the Fermi surface may occur, resulting in a sudden transition from SC-I to SC-II.

As seen from Fig. 5(c), the T_c values for the low-T_c and high-T_c phases are completely separated in the c range of the SC-I and SC-II phase of $(NH_3)_yCs_xFeSe$, i.e., both phases of $(NH_3)_yNa_xFeSe$ do not cross the c value of ~14.0 Å, which corresponds to the c value providing the transition from SC-I to SC-II in $(NH_3)_yCs_xFeSe$. If the Lifshitz transition is related to the shrinkage of the lattice, and its critical point is the above

c value, no transition of SC-I to SC-II in $(NH_3)_yNa_xFeSe$ can be reasonably understood. If this is the case, then to achieve the transition of SC-I to SC-II (or pressure-driven high-T_c phase), more pressure must be applied for the high-T_c phase of $(NH_3)_yNa_xFeSe$ to reach the critical c value (14.0−14.2 Å).

In Fig. 6, the precise T_c-c phase diagram is drawn for M_xFeSe. The T_c could be smoothly scaled with the c (or FeSe plane spacing), and a discontinuous jump is present between SC-I and SC-II. The T_c-c plot for the low-T_c phase overlaps with that of SC-II in $(NH_3)_yCs_xFeSe$. Further expansion of c above 17.5 Å provides a negative pressure effect on T_c in M_xFeSe. Here, we suggest a unified scenario to explain these results. The increase in 2D caused by extension of c improves the Fermi surface nesting to enhance spin fluctuation, which may reinforce the electron pairing to increase the T_c. This has been suggested for metal-doped HfNCl [27]. Further expansion of the FeSe plane spacing acts against superconductivity in metal-doped FeSe, because of the reduced interaction between FeSe layers (FeSe layer coupling). Such a suppression of T_c with greater FeSe-plane separation is observed in metal-doped HfNCl [27]. Recently, Kuroki *et al.* suggested that the superconductivity is optimized when Fermi surface nesting is degraded to some extent [36], which allows finite energy spin fluctuations around the nesting vector to develop. This may explain the existence of an optimum FeSe plane spacing for superconductivity.

V. CONCLUSION AND OUTLOOK

The T_c-c phase diagram for the metal-doped FeSe system was drawn based on the pressure dependence of the low-T_c and high-T_c phases in $(NH_3)_yNa_xFeSe$ produced in this study, and the previous reports on physical and chemical pressure effects in metal-doped FeSe [20–22,24,25,29–31]. The T_c-c plot shows two different linear relationships below $c = 17.5$ Å, which belong to the SC-I and SC-II range of $(NH_3)_yCs_xFeSe$ [19]. A discontinuous jump of T_c against c was found for $(NH_3)_yCs_xFeSe$, which may originate in a Lifshitz transition due to the change of the topology of the Fermi surface, from the analogy to $(NH_3)_yLi_xFeSe$ [26]. If we assume that the Lifshitz transition may occur universally at $c \sim 14$ Å in M_xFeSe, no transition of SC-I to SC-II in the high-T_c and low-T_c phases of $(NH_3)_yNa_xFeSe$ may be attributed to the scenario that the Lifshitz transition does not appear because the c values of both phases do not pass through $c \sim 14$ Å, as seen from Fig. 5(c), although direct evidence that Lifshitz transition occurs at $c = 14$ Å is not still obtained.

In addition, it may be reasonable to comment that the pressure-driven transition may be observed if we can synthesize a $(NH_3)_yNa_xFeSe$ sample with a suitable lattice constant c, i.e., a c value that is closer to 14 Å. This may provide direct evidence for the significance of $c = 14$ Å as a critical value in the transition of SC-I to SC-II. However, it is impossible to synthesize such a $(NH_3)_yNa_xFeSe$ sample because $(NH_3)_yNa_xFeSe$ phases with only two different c values can be realized, even if x is varied, as evidenced by our previous report [22]. In this study, we did not comment on the role of the AFM phase in the transition of SC-I to SC-II, because the samples used were polycrystalline powders; it is difficult to detect the presence of an AFM phase in case of the polycrystalline powder sample.

The increase in T_c with c implies that improvement of Fermi surface nesting leads to the strengthening of electron pairing, as evidenced in metal-doped HfNCl [27,28]. The T_c then slowly decreases as c values increase above 17.5 Å, and approaches the ∼40 K realized by electrostatic electron doping of FeSe on $SrTiO_3$ [32], which is 2D superconductivity. The disappearance of layer coupling has a negative effect on superconductivity, and the limit of T_c achievable by separating the FeSe layers is expected to be ∼40 K. Thus the fact that no transition of SC-I to SC-II was found for the two phases of $(NH_3)_yNa_xFeSe$ treated in this study led to the systematic understanding of the T_c-c phase diagram of M_xFeSe.

ACKNOWLEDGMENTS

Y.K. greatly appreciates the valuable comments offered on this study by Yoji Koike of Tohoku University. This study was partly supported by Grants-in-Aid (26105004 and 26400361) from MEXT, by JST ACT-C Grant No. JPMJCR12YW, Japan, and by the Program for Promoting the Enhancement of Research Universities. The XRD measurements at SPring-8 were supported by 2016B4126 and 2016B4131.

[1] L. Sun, X.-J. Chen, J. Guo, P. Gao, Q.-Z. Huang, H. Wang, M. Fang, X. Chen, G. Chen, Q. Wu, C. Zhang, D. Gu, X. Dong, L. Wang, K. Yang, A. Li, X. Dai, H.-K. Mao, and Z. Zhao, Re-emerging superconductivity at 48 kelvin in iron chalcogenides, Nature (London) **483**, 67 (2012).

[2] J. Guo, X.-J. Chen, J. Dai, C. Zhang, J. Guo, X. Chen, Q. Wu, D. Gu, P. Gao, L. Yang, K. Yang, X. Dai, H.-k. Mao, L. Sun, and Z. Zhao, Pressure-Driven Quantum Criticality in Iron-Selenide Superconductors, Phys. Rev. Lett. **108**, 197001 (2012).

[3] V. Ksenofontov, S. A. Medvedev, L. M. Schoop, G. Wortmann, T. Palasyuk, V. Tsurkan, J. Deisenhofer, A. Loidl, and C. Felser, Superconductivity and magnetism in $Rb_{0.8}Fe_{1.6}Se_2$ under pressure, Phys. Rev. B **85**, 214519 (2012).

[4] P. Gao, R. Yu, L. Sun, H. Wang, Z. Wang, Q. Wu, M. Fang, G. Chen, J. Guo, C. Zhang, D. Gu, H. Tian, J. Li, J. Liu, Y. Li, X. Li, S. Jiang, K. Yang, A. Li, Q. Li, and Z. Zhao, Role of 245 phase in alkaline iron selenide superconductors revealed by high-pressure studies, Phys. Rev. B **89**, 094514 (2014).

[5] D. Gu, Q. Wu, Y. Zhou, P. Gao, J. Guo, C. Zhang, S. Zhang, m S. Jiang, K. Yang, A. Li, L. Sun, and Z. Zhao, Superconductivity in pressurized $Rb_{0.8}Fe_{2-y}Se_{2-x}Te_x$, New J. Phys. **17**, 073021 (2015).

[6] H. Okabe, N. Takeshita, K. Horigane, T. Muranaka, and J. Akimitsu, Pressure-induced high-T_c superconducting phase in FeSE: correlation between anion height and T_c, Phys. Rev. B **81**, 205119 (2010).

[7] Y. Zhou, X. Chen, R. Zhang, J. Shao, X. Wang, C. An, Y. Zhou, C. Park, W. Tong, L. Pi, Z. Yang, C. Zhang, and Y. Zhang, Pressure-induced reemergence of superconductivity in topological insulator $Sr_{0.065}Bi_2Se_3$, Phys. Rev. B **93**, 144514 (2016).

[8] P. P. Kong, J. L. Zhang, S. J. Zhang, J. Zhu, Q. Q. Liu, R. C. Yu, Z. Fang, C. Q. Jin, W. G. Yang, X. H. Yu, J. L. Zhu, and Y. S. Zhao, Superconductivity of the topological insulator Bi_2Se_3 at high pressure, J. Phys.: Condens. Matter **25**, 362204 (2013).

[9] Y. Qi, P. G. Naumov, N. A. Mazhar, C. R. Rajamathi, W. Schnelle, O. Baralov, M. Hanfland, S.-C. Wu, C. Shekhar, Y. Sun, V. Suβ, M. Schmidt, U. Schwarz, E. Pippel, P. Werner, R. Hillebrand, T. Förster, E. Kampert, S. Parkin, R. J. Cava, C. Felser, B. Yan, and S. A. Medvedev, Superconductivity in weyl semimetal candidate $MoTe_2$, Nat. Commun. **7**, 11038 (2016).

[10] X.-C. Pan, X. Chen, H. Liu, Y. Feng, Z. Wei, Y. Zhou, Z. Chi, L. Pi, F. Yen, F. Somg, X. Wan, Z. Yang, B. Wang, G. Wang, and Y. Zhang, Pressure-driven dome-shaped superconductivity and electronic structural evolution in tungsten ditelluride, Nat. Commun. **6**, 7805 (2015).

[11] J. Guo, S. Jin, G. Wang, S. Wang, K. Zhu, T. Zhou, M. He, and X. Chen, Superconductivity in the iron selenide $K_xFe_2Se_2$ ($0 \leqslant x \leqslant 1.0$), Phys. Rev. B **82**, 180520(R) (2010).

[12] A. F. Wang, J. J. Ying, Y. J. Yan, R. H. Liu, X. G. Luo, Z. Y. Li, X. F. Wang, M. Zhang, G. J. Ye, P. Cheng, Z. J. Xiang, and X. H. Chen, Superconductivity at 32 k in single-crystalline $Rb_xFe_{2-y}Se_2$, Phys. Rev. B **83**, 060512(R) (2011).

[13] A. Krzton-Maziopa, Z. Shermadini, E. Pomjakushina, V. Pomjakushin, M. Bendele, A. Amato, R. Khasanov, H. Luetkens, and K. Conder, Synthesis and crystal growth of $Cs_{0.8}(FeSe_{0.98})_2$: A new iron-based superconductor with $T_c = 27$ K, J. Phys.: Condens. Matter **23**, 052203 (2011).

[14] M.-H. Fang, H.-D. Wang, C.-H. Dong, Z. Luan, C.-M. Feng, J. Chen, and H. Q. Yuan, Fe-based superconductivity with $T_c =$ 31 K bordering an antiferromagnetic insulator in (Tl,K)Fe_xSe_2, EPL **94**, 27009 (2011).

[15] W. Li, H. Ding, P. Deng, K. Chai, C. Song, K. He, L. Wang, X. Ma, J.-P. Hu, X. Chen, and Q.-K. Xue, Phase separation and magnetic order in K-doped iron selenide superconductor, Nat. Phys. **8**, 126 (2012).

[16] H.-H. Wen, Overview on the physics and materials of the new superconductor $K_xFe_{2-y}Se_2$, Rep. Prog. Phys. **75**, 112501 (2012).

[17] Y. Liu, Q. Xiang, K. W. Dennis, R. W. McCallum, and T. A. Lograsso, Evolution of precipitate morphology during heat treatment and its implications for the superconductivity in $K_xFe_{1.6+y}Se_2$ single crystals, Phys. Rev. B **86**, 144507 (2012).

[18] X. Ding, D. Fang, Z. Wang, H. Yang, J. Liu, Q. Ding, G. Ma, C. Meng, Y. Hu, and H.-H. Wen, Influence of microstructure on superconductivity in $K_xFe_{2-y}Se_2$ and evidence for a new parent phase $K_2Fe_7Se_8$, Nat. Commun. **4**, 1897 (2013).

[19] M. Izumi, L. Zheng, Y. Sakai, H. Goto, M. Sakata, Y. Nakamoto, H. L. T. Nguyen, T. Kagayama, K. Shimizu, S. Araki, T. C. Kobayashi, T. Kambe, D. Gu, J. Guo, Y. Li, L. Sun, K. Prassides, and Y. Kubozono, Emergence of double-dome superconductivity in ammoniated metal-doped FeSe, Sci. Rep. **5**, 9477 (2015).

[20] L. Zheng, M. Izumi, Y. Sakai, R. Eguchi, H. Goto, Y. Takabayashi, T. Kambe, T. Onji, S. Araki, T. C. Kobayashi, J. Kim, A. Fujiwara, and Y. Kubozono, Superconductivity in $(NH_3)_yCs_xFeSe$, Phys. Rev. B **88**, 094521 (2013).

[21] T. P. Ying, X. L. Chen, G. Wang, S. F. Jin, T. T. Zhou, X. F. Lai, H. Zhang, and W. Y. Wang, Observation of superconductivity at $30 \sim 46$ K in $A_xFe_2Se_2$ (A = Li, Na, Ba, Sr, Ca, Yb, and Eu), Sci. Rep. **2**, 426 (2012).

[22] L. Zheng, X. Miao, Y. Sakai, M. Izumi, S. Nishiyama, E. Uesugi, Y. Kasahara, Y. Iwasa, and Y. Kubozono, Emergence of multiple superconducting phases in $(NH_3)_yM_xFeSe$ (M: Na and Li), Sci. Rep. **5**, 12774 (2015).

[23] J. Guo, H. Lei, F. Hayashi, and H. Hosono, Superconductivity and phase instability of NH3-free Na-intercalated $FeSe_{1-z}Te_z$, Nat. Commun. **5**, 4756 (2014).

[24] L. Zheng, Y. Sakai, X. Miao, S. Nishiyama, T. Terao, R. Eguchi, H. Goto, and Y. Kubozono, Superconductivity in $(NH_3)_yNa_xFeSe_{0.5}Te_{0.5}$, Phys. Rev. B **94**, 174505 (2016).

[25] X. Miao, T. Terao, X. Yang, S. Nishiyama, T. Miyazaki, H. Goto, Y. Iwasa, and Y. Kubozono, Preparation of new superconductors by metal doping of two-dimensional layered materials using ethylene diamine, Phys. Rev. B **96**, 014502 (2017).

[26] P. Shahi, J. P. Sun, S. S. Sun, Y. Y. Jiao, K. Y. Chen, S. H. Wang, H. C. Lei, Y. Uwatoko, B. S. Wang, and J.-G. Cheng, High-T_c superconductivity up to 55 K under high pressure in the heavily electron doped $Li_x(NH_3)_yFe_2Se_2$ single crystal, Phys. Rev. B **97**, 020508 (2018).

[27] T. Takano, T. Kishiume, Y. Taguchi, and Y. Iwasa, Interlayer-Spacing Dependence of T_c in Li_xM_yHfNCl (M: Molecule) Superconductors, Phys. Rev. Lett. **100**, 247005 (2008).

[28] G. Ye, J. Ying, Y. Yan, X. Luo, P. Cheng, Z. Xiang, A. Wang, and X. Chen, Superconductivity in Yb_xM_yHfNCl (M: Molecule) superconductors, Phys. Rev. B **86**, 134501 (2012).

[29] T. Hatakeda, T. Noji, T. Kawamata, M. Kato, and Y. Koike, New Li-ethylenediamine-intercalated superconductor $Li(C_2H_8N_2)_yFe_{2-z}Se_2$ with $T_c = 45$ K, J. Phys. Soc. Jpn. **82**, 123705 (2013).

[30] T. Noji, T. Hatakeda, S. Hosono, T. Kawamata, M. Kato, and Y. Koike, Synthesis and post-annealing effects of alkaline-metal-ethylenediamine- intercalated superconductors $A_x(C_2H_8N_2)_yFe_{2-z}Se_2$(A = Li, Na) with $T_c = 45$ K, Physica C **504**, 8 (2014).

[31] S. Hosono, T. Noji, T. Hatakeda, and T. Kawamata, M. Kato, and Y. Koike, New superconducting phase of $Li_x(C_6H_{16}N_2)_yFe_{2-z}Se_2$ with $T_c = 41$ K obtained through the post-annealing, J. Phys. Soc. Jpn. **85**, 013702 (2016).

[32] J. Shiogai, Y. Ito, T. Mitsuhashi, T. Nojima, and A. Tsukazaki, Electric-field-induced superconductivity in electrochemically etched ultrathin FeSe films on $SrTiO_3$ and MgO, Nat. Phys. **12**, 42 (2016).

[33] Y. Yamamoto, H. Yamaoka, S. Onari, M. Yoshida, N. Hirao, S. Kawaguchi, Y. Oishi, X. Miao, Y. Kubozono, J.-F. Lin, N. Hiraoka, H. Ishii, Y.-F. Liao, K.-D. Tsuei, and J. Izuki (unpublished).

[34] M. Ren, Y. Yan, X. Niu, R. Tao, D. Hu, R. Peng, B. Xie, J. Zhao, T. Zhang, and D.-L. Feng, Superconductivity across lifshitz transition and anomalous insulating states in surface K-dosed $(Li_{0.8}Fe_{0.2}OH)FeSe$, Sci. Adv. **3**, e1603238 (2017).

[35] T. Shiroka, T. Shang, C. Wang, G.-H. Gao, I. Eremin, H.-R. Ott, and J. Mesot, High-T_c superconductivity in undoped ThFeAsN, Nat. Commun. **8**, 156 (2017).

[36] M. Kuroki, D. Ogura, H. Usui, and K. Kuroki, Finite-energy spin fluctuation pairing glue in systems with coexisting electron and hole bands, Phys. Rev. B **95**, 214509 (2017).